Annals of Nuclear Energy 38 (2011) 1144–1155

Contents lists available at ScienceDirect

Annals of Nuclear Energy

journal homepage: www.elsevier.com/locate/anucene

# Optimal ion beam, target type and size for accelerator driven systems: Implications to the associated accelerator power

S.R. Hashemi-Nezhad [a,*], W. Westmeier [b], M. Zamani-Valasiadou [c], B. Thomauske [d], R. Brandt [b]

[a] Institute of Nuclear Science, School of Physics, A28, University of Sydney, NSW 2006, Australia
[b] Institut für Kernchemie, Philipps-Universität, 35032 Marburg, Germany
[c] Aristotle University, Thessaloniki, Greece
[d] Forschungszentrum Jülich, ISR-6, 52425 Jülich, Germany

ARTICLE INFO

*Article history:*
Received 21 April 2010
Received in revised form 29 November 2010
Accepted 9 December 2010
Available online 8 January 2011

*Keywords:*
Accelerator driven systems
Energy gain
Target types
Optimal target size
ADS power
MCNPX code

ABSTRACT

In interactions of different energetic ions with extended targets hydrogen isotopes are the most effective projectiles for the production of spallation neutrons. It is shown that for every target material and incident ion type and energy there is an optimal target size which results in the escape of a maximum number of spallation neutrons from the target. Calculations show that in an ADS, combination of a beam of 1.5 GeV deuteron projectiles and a uranium target results in the highest neutron production rate and therefore highest energy gain. For fast 1.5 GeV d + $^{238}$U ADS with lead or lead–bismuth eutectic moderator, the required ion beam current is only 38% of that for 1 GeV proton projectiles on lead target. It is shown that for a modular ADS with uranium target and output power of 550 $MW_{th}$ a 1.5 GeV deuteron beam of current 1.8 mA is required, which is easily achievable with today's technology. For an ADS with $k_{eff}$ = 0.98 and output power of 2.2 $GW_{th}$, the required beam currents for (a) 1 GeV p + Pb and (b) 1.5 GeV d + U systems are 18.5 and 7.1 mA, respectively.



## 1. Introduction

The term accelerator driven system (ADS) refers to a sub-critical nuclear assembly, which is coupled to an accelerator. In an ADS the nuclear chain reaction is sustained by spallation neutrons (Barashenkov et al., 1974; Carminati et al., 1993) produced via interaction of energetic ions, e.g. protons with an extended massive target (such as lead). An ADS with adequate output power can be used for nuclear energy generation as well as in transmutation of nuclear waste isotopes (Adam et al., 2002; Bowman et al., 1992; Hashemi-Nezhad et al., 2002; Rubbia et al., 1997). The output power of an ADS depends on the extent of the subcriticality of the system $k_{eff}$[1] (the effective neutron multiplication factor) and the spallation neutron yield per unit time. The latter depends on the type of the target, the ion, the ion energy, as well as on the average ion beam current of the attached accelerator.

It is shown that for a sub-critical system with $k_{eff}$ = 0.98 and thermal output power of 1500 $MW_{th}$ a 1 GeV proton beam of average current 12.5 mA is required (Fernandez et al., 1996; Rubbia et al., 1995). Such a beam current is equivalent to a thermal power of 12.5 $MW_{th}$.

Some of the technological challenges that one faces in realization of an industrial scale ADS are: (a) the construction of a high-power ion accelerator, (b) providing solutions to the problems associated with the stability of the accelerator beam window and (c) heat extraction from and cooling of the target.

It is highly desirable to reduce the beam power while maintaining the required output power of the ADS. To achieve this goal one needs to increase the power gain of the system (i.e. power output per unit energy of the incident ion). This could be achieved by increasing the neutron yield per ion and per unit energy deposited in the system, through optimal selections of (i) the ion type for acceleration, (ii) the ion energy, (iii) the target material and (iv) the target size.

## 2. Monte Carlo calculations

In this work all Monte Carlo calculations were performed using the MCNPX 2.7a code (Pelowitz et al., 2008). The high-energy data libraries for neutron and proton interactions (Chadwick et al., 1999) were used where they were available.

In the MCNPX code, (Bertini, 1963, 1969), ISABEL (Yariv and Fraenkel, 1979, 1981), INCL4 (Boudard et al., 2002) intranuclear

* Corresponding author. Tel.: +61 2 93515964; fax: +61 2 93517726.
*E-mail address:* reza@physics.usyd.edu.au (S.R. Hashemi-Nezhad).

[1] $k_{eff}$ is the effective neutron multiplication factor, obtained in absence of neutron source and is based on the fission neutrons with Watt spectrum.

0306-4549/$ - see front matter © 2010 Elsevier Ltd. All rights reserved.
doi:10.1016/j.anucene.2010.12.008

**Table 1**
Neutron yield calculated using different INC, evaporation and fission models, available in the MCNPX code. A lead target of radius 10 cm and length 60 cm was irradiated with 1 GeV proton beam of diameter 1 cm.

| $j$ | Model combinations used in the calculations | Lead target | | Uranium target | |
|---|---|---|---|---|---|
| | | $(n_{Pb})_j$ | $[(n_{Pb})_j - (n_{Pb})_1]/(n_{Pb})_1$ (%) | $(n_U)_j$ | $[(n_U)_j - (n_U)_1]/(n_U)_1$ (%) |
| 1 | Bertini/Dresner | 23.3 | 0.0 | 48.9 | 0.0 |
| 2 | ISABEL/Dresner | 22.9 | −1.7 | 47.7 | −2.5 |
| 3 | Bertini/ABLA | 24.4 | 4.7 | 52.2 | 6.7 |
| 4 | ISABEL/ABLA | 24.0 | 3.0 | 51.6 | 5.5 |
| 5 | INCL4/Dresner | 21.3 | −8.6 | 46.5 | −4.9 |
| 6 | INCL4/ABLA | 22.3 | −4.3 | 49.9 | 2.0 |
| 7 | CEM03 | 23.9 | 2.6 | 54.9 | 12.3 |

cascade (INC) models and an old version of Fluka high-energy generator[2] (Aarnio et al., 1986) are available. These models can be used in combination with Dresner evaporation model (Dresner, 1981), ABLA evaporation–fission model (Junghans et al., 1998), RAL (Atchison, 1980) and ORNL (Barish et al., 1981) fission models. Moreover CEM03 (Mashnik et al., 2006) a self-contained INC and evaporation–fission code is also available; refer to (Pelowitz, 2008) for details.

To compare the neutron multiplicities predicted by these models, neutron yields from $^{nat}$Pb and $^{238}$U-targets of diameter 20 cm and length 60 cm were calculated when they were irradiated with 1 GeV proton beam of diameter 1 cm parallel to the target axis. Calculations were made for different INC, evaporation and fission model combinations as shown in Table 1. In all calculations involving the Dresner evaporation model the RAL fission model also was used. In Table 1, $j$ refers to the model combinations used in the calculations and $(n_{Pb})_j$ and $(n_U)_j$ are the neutron multiplicities for the Pb and U-targets, respectively. The column next to neutron multiplicity of each target, gives the deviation of the neutron yield from that predicted by Bertini/Dresner. For all model calculations the deviation is less than 9% except for the case of CEM03 where it is ~12% for the uranium target. Further investigations showed that the excess neutron multiplicity predication by CEM03 for the U-target is due to overestimation of fission events for high-energy interactions predicted by this model as compared to the others.

Fig. 1 shows the experimental and calculated neutron yields from a $^{nat}$Pb-target of diameter 20 cm and length 60 cm as a function of incident proton energy ($E_p$). The MC calculations were performed using the Bertini/Dresner models. Fig. 1a shows the calculated total neutron multiplicities which are in agreement (within the experimental uncertainties) with the experimental results of (Yurevich, 2010; Yurevich et al., 2006).

Fig. 1b illustrates the calculated and experimental (Vassilkov et al., 1995) yield of spallation neutrons with energy less than 15 MeV for incident protons of energies less than 4 GeV. The (Vassilkov et al., 1995) experimental neutron yields are consistently less than those of the calculation. The deviation is about 12% at $E_p$ = 3.66 GeV and less than 9% at $E_p \leqslant 2$ GeV.

In this paper we used the Bertini intranuclear cascade, Dresner evaporation and RAL fission models in all calculations. Neutron multiplicity predictions by these models, at the projectile energies considered in this paper, are in satisfactory agreement with the experiments as discussed above. A possible deviation of less than 10% between the experimental and calculated neutron multiplicities will not alter the conclusions of this paper.

## 3. Ion types

In order to determine which ions are most effective in production of spallation neutrons, neutron yields for interactions of different ions (from proton to lead) having energy of 1 AGeV with an extended lead target were calculated. The target had a diameter of 20 cm and length of 170 cm. The length of the target was chosen to be longer than the range of the most penetrating ions in lead. In this case the length was chosen on the basis of the total range of 1 AGeV triton ions in lead (163 cm) as calculated using the SRIM code (Ziegler et al., 1985). In the calculations the target was irradiated with cylindrical ion beams of diameter 1 cm parallel to the target axis. At this stage the target diameter was chosen rather arbitrarily (the optimal target diameter will be discussed in other parts of this paper). We define the neutron production rate (NPR) as $\chi = \frac{Y}{E_i}$ where $Y$ is the neutron yield per incident ion and $E_i$ is the total kinetic energy of the ion expressed in units of GeV.

Two groups of neutron yields were calculated

1. Sum of the neutrons produced in the intranuclear cascade (INC), Pre-equilibrium and evaporation stages of the interaction as well as possible fission events of the excited residual nuclei left-over from the nuclear processes beyond the INC, $Y_i$, for which NPR is, $\chi_i$. This is expected to be independent of the target size as long as the target length is longer than the range of the ion of interest in the target material.
2. Total neutron yield $Y_t$ which includes $Y_i$ plus neutrons produced in the course of inter-nuclear cascades. Total NPR for this case is $\chi_t$.

Fig. 2a and b show the variation of the NPR as a function of total kinetic energy of ions. From these figure it is evident that:

1. Although the number of neutrons for a given ion in Fig. 2a and b are different the shapes of the plots for $\chi_i$ and $\chi_t$ is the same. This implies that, at least in the case of the Pb-target, inclusion of the neutrons from the inter-nuclear cascade do not significantly alter the shape of the Fig. 2a.
2. The neutron production rate is highest for projectiles of hydrogen isotopes. The values of the $\chi_t$ for proton, deuteron and triton are 24.42, 26.83 and 27.14, respectively.

## 4. Target types

Neutron yield at incident proton energy of 1 GeV was calculated for some metallic target materials of diameter 20 cm and length 170 cm, when protons strike cylindrical targets parallel to their axis (Fig. 3). To treat all target materials equally, in Fig. 3 we deliberately have not included the neutrons resulting from secondary neutron induced fissions in the target material. This is because; the secondary neutron induced fission rate depends on the target size and will affect the neutron multiplicities of the uranium and thorium targets significantly. Moreover the MC code produces the secondary neutron induced fission contributions to the neutron multiplicity only for the uranium and thorium targets and not for the other materials shown in Fig. 3.

[2] Latest version of Fluka code is available from; http://www.fluka.org/fluka.php.

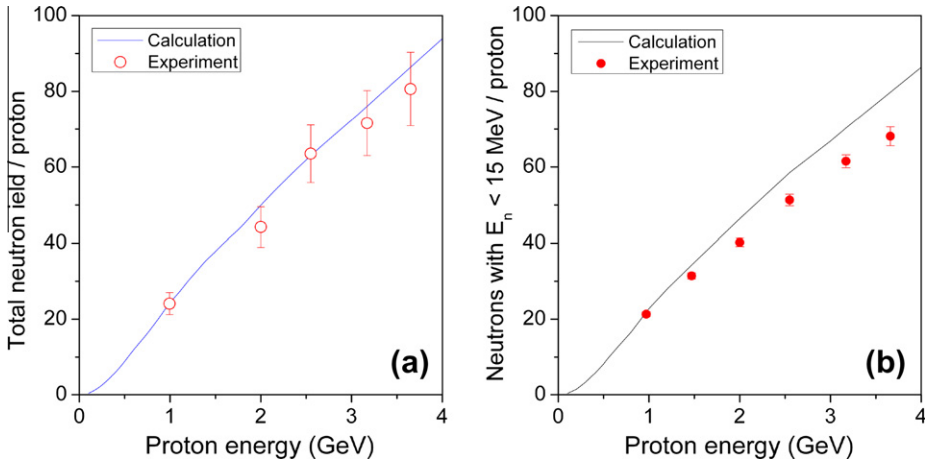


**Fig. 1.** MC and experimental results on neutron multiplicity on interaction of protons of different energies with a lead target of diameter 20 cm and length 60 cm. (a) Total neutron yield, experimental data are from (Yurevich, 2010; Yurevich et al., 2006). (b) Neutrons of energy less than 15 MeV, experimental data are from (Vassilkov et al., 1995).

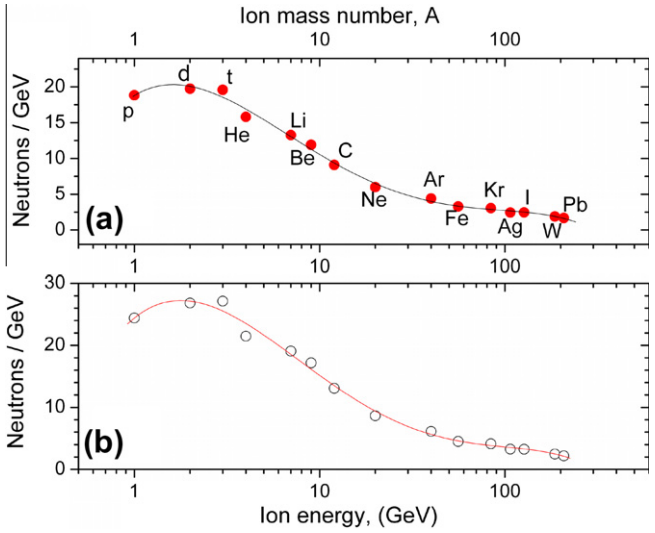


**Fig. 2.** Variations of neutron production rates as a function of incident ion energy in interaction of different ions with a lead target of diameter 20 cm and length 170 cm. The data shown refer to hydrogen isotopes (p, d and t) and ions of $^{4}$He, $^{7}$Li, $^{9}$Be, $^{12}$C, $^{20}$Ne, $^{40}$Ar, $^{56}$Fe, $^{84}$Kr, $^{107}$Ag, $^{127}$I, $^{184}$W and $^{208}$Pb. (a) NPR $\chi_i$ due to neutrons produced in intranuclear cascade, pre-equilibrium and evaporation stages of the reaction. (b) Total NPR, $\chi_t$.

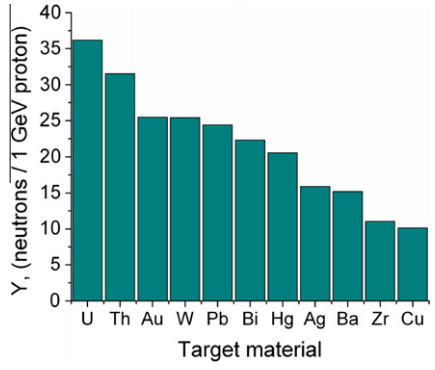


**Fig. 3.** Neutron yield at incident proton energy of 1 GeV for some metallic target materials of diameter 20 cm and length 170 cm. Neutron from the secondary neutron induced fission events in the target are not included.

From these we investigate four target materials $^{238}$U, $^{232}$Th, $^{nat}$Pb and $^{nat}$W. Some of the physical and neutronic characteristics of the chosen target materials are given in Table 2.

Calculations show that the neutron yield from $^{nat}$Pb-target is only ~0.16% higher than that from a lead–bismuth eutectic (LBE) target (44.5 wt.% Pb + 55.5 wt.% Bi), (NEA, 2007).

## 5. Neutron yields in interactions of protons and deuterons with extended metallic targets

As already mentioned, hydrogen isotopes are the most effective projectiles for the production of spallation neutrons. In this work two non-radioactive isotopes of hydrogen will be considered as projectiles for an ADS.

Neutron yields in interactions of protons and deuterons of different energies with cylindrical $^{nat}$W, $^{nat}$Pb, $^{232}$Th and $^{238}$U-targets of diameter 20 cm and length 170 cm were calculated. Results are shown in Fig. 4.

From these calculations we reach the following conclusions;

1. For all targets NPR increases sharply with increasing projectile energy reaching a maximum beyond which it decreases at a much slower rate. The relative reduction in the NPR beyond the maximum is more pronounced for W-, Th- and U-targets than for Pb-target.
2. NPRs for deuteron projectiles are higher than those for protons of the same energy, for all target materials. Similar results have been obtained (Ridikas and Mittig, 1998) using the LCS-code system (Prael and Lichtenstein, 1989).
3. The maximum neutron production rate appears at energy of ~1.5 GeV for all four targets studied in this paper although such a maximum NPR is not that obvious in the case of the proton interaction with Pb-target.
4. Neutron yield is strongly dependent on the target size (Hashemi-Nezhad et al., 2001; Lone and Wong, 1995) and Fig. 4 may suggest that the reduction in NPR at high projectile energies may be attributed to ratio of the target length and the ion range in the target material. The relevance of such an argument to the irradiation conditions used in this work will become clearer in the following.

In Fig. 5 the NPR for U-target is plotted against the range of incident ions in the target material (the length of the target is shown in the inset of the figure). It can be seen that reduction in NPR starts at projectile energies for which the range of the ions is ~25% of the

**Table 2**
Some physical and neutronic characteristics of the target materials studied.

| Target type | Density (g cm$^{-3}$) | Melting point (°C) | Fissionability | Fertile | Neutron absorption cross-section |
|---|---|---|---|---|---|
| $^{238}$U | 19.04 | 1132 | High | Yes | High |
| $^{232}$Th | 11.66 | 1842 | High | Yes | High |
| $^{nat}$Pb | 11.34 | 327 | Very low | No | Low |
| $^{nat}$W | 19.35 | 3422 | Very low | No | High |
| LBE[a] | 10.5 | ~124 | Very low | No | Low |

[a] 44.5 wt.% Pb + 55.5 wt.% Bi (NEA, 2007).

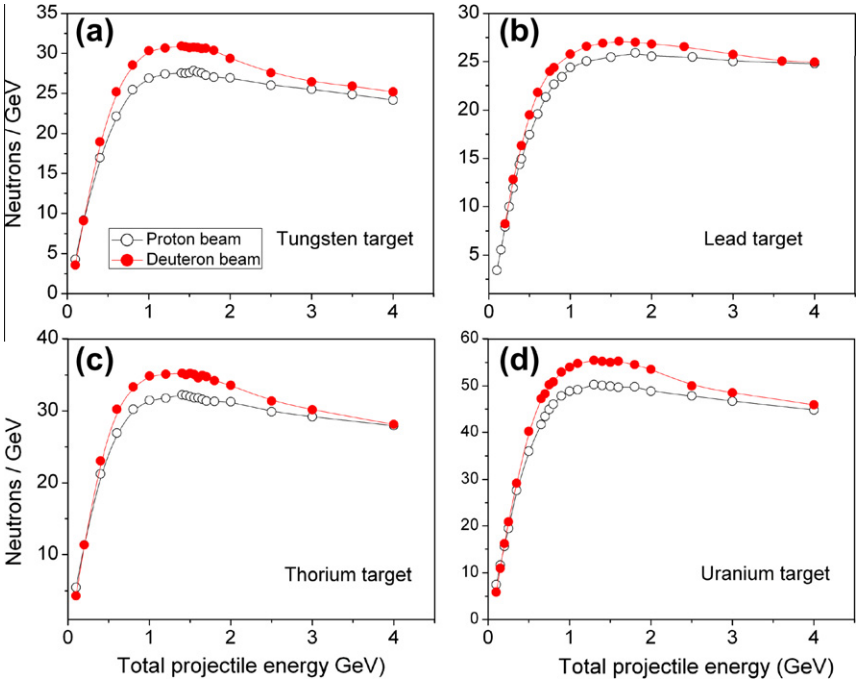


**Fig. 4.** Variation of neutron production rate (NPR) as a function of incident ion energy (proton or deuteron) in interactions with tungsten, lead, thorium, and uranium targets. The cylindrical targets had diameter 20 cm and length 170 cm.

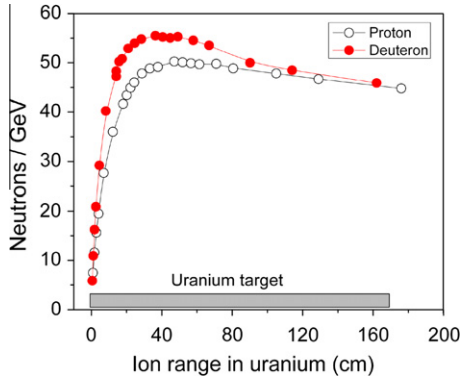


**Fig. 5.** Neutron production rate as a function of range of the incident ions in the uranium target. (The length of the target is shown in the figure inset.)

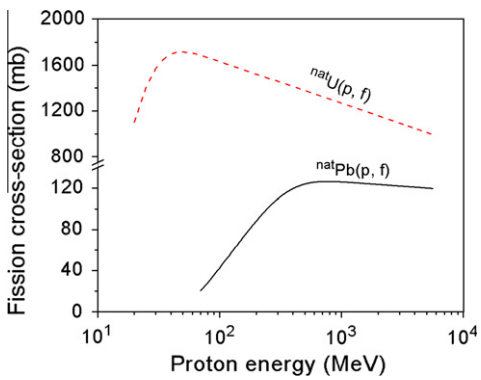


**Fig. 6.** Energy dependent proton induced fission cross-sections of natural uranium and lead. The cross-section values were obtained using the systematics given by (Prokofiev, 2001b).

target length. Thus the reduction of NPR with increasing ion energy beyond the maximum NPR does not result from the target size (for the energy range and the irradiation geometry investigated in this paper). Instead it is consequence of the reduction in the interaction cross-section of the projectile with the target nuclei. As an example, in Fig. 6 the energy dependence of proton induced fission cross-sections in natural lead and natural uranium targets is shown. The cross-section values were obtained using the systematics given by (Prokofiev, 2001b). With increasing proton energy, the Pb(p, f) cross-section beyond its maximum (at ~765 MeV) reduces much more slowly with increasing proton energy than the U(p, f) cross-section beyond its maximum (at ~65 MeV).

In this paper we will compare an ADS driven by 1 GeV protons (a widely accepted proton energy for an industrial scale ADS, see e.g. Andriamonje et al., 1995) with the case when it is driven by 1.5 GeV deuterons (corresponding to the energy where maximum NPR is achieved (Fig. 4)).

## 6. Determination of optimal spallation neutron target sizes

### 6.1. Definition of spallation neutron source

In an ADS only those neutrons that escape the target and enter the ADS volume are important but not the total neutron yield in the interaction of the incident ions with the target nuclei. Only the escaping neutrons can participate in neutron multiplication via fission and contribute to the power generation in the system.

Therefore we define the source neutrons as those that escape the target volume and are produced by interactions of the primary ions (spallation reactions) and resulting secondary particles with the target nuclei (inter-nuclear cascades). With this definition the neutrons resulting from fission events induced by secondary particles in the target nuclei (prior to their exit from the target volume), will contribute to the source neutron intensity. Once neutrons exit the target they will be considered as part of the neutron field of the ADS and their possible re-entry into target and further interactions with the target nuclei will be treated similar to any other neutron in the system. With this definition the optimal target size refers to the target dimensions which for a given incident ion and its energy, results in leakage of largest number of neutrons from the target surfaces.

The neutron production rates shown in Fig. 4 refer to total neutron yields and are the sum of the neutrons that escape from and those that are absorbed in the target.

Both the neutron production and absorption rates depend on the target size. Neutron production increases with the target size until it reaches a plateau value (Hashemi-Nezhad et al., 2001) and neutron absorption increases continuously with the target size until all produced neutrons are absorbed. Therefore, for a given ion, energy and target material there must be optimum target dimensions and geometry that results in maximum neutron leakage from the target. The extent of the neutron leakage from a target strongly depends on the energy dependent neutron absorption cross-section $\sigma_a(E)$, of the target nuclei. In Fig. 7 we show $\sigma_a(E)$ as a function of energy for $^{nat}$W, $^{208}$Pb, $^{232}$Th, and $^{238}$U. At energies less than ~10 keV the $\sigma_a(E)$ for W, Th and U are more than ~4 orders of magnitude higher than that of Pb.

### 6.2. Irradiations with 1 GeV protons

To investigate the effects of the $\sigma_a(E)$ on the number of the neutrons that escape the target, the following calculations were performed;

1. Cylindrical tungsten, lead, thorium and uranium targets of radius 10 cm were irradiated with 1 GeV protons and number of neutrons that escape the target, those that are absorbed in the target, and the total neutron yield were calculated. Calculations were performed for different target length in the range of 1 cm to 120 cm (more than twice of the range of 1 GeV protons in the target materials). The inelastic interaction mean free path $\lambda_{in}$ for 1 GeV protons is 16.5 cm in lead and 10.5 cm in uranium. Thus the target length is a factor of ~16 and ~10 greater than the $\lambda_{in}$, for uranium and lead targets, respectively.

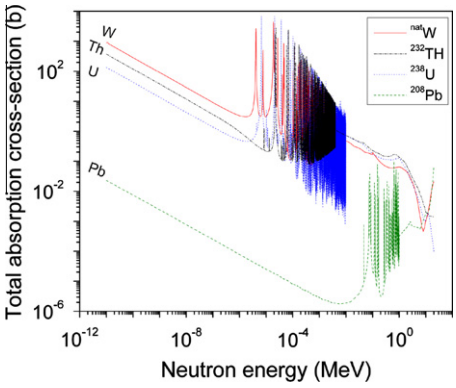


**Fig. 7.** Total absorption cross-section of W (ENDF/B-6.1), $^{208}$Pb (ENDF/B-6.0), $^{232}$Th (ENDF/B-6.0) and $^{238}$U (ENDF/B-6.2).

These calculations illustrate that in the case of all four target materials, the numbers of leakage and absorbed neutrons (and therefore total neutron yield) reach a saturation value at target lengths greater than the range of the projectile in the target material.

2. Cylindrical tungsten, lead, thorium and uranium targets of length slightly longer than the range of the 1 GeV protons in the targets were irradiated with protons of energy 1 GeV parallel to their axis. The number of the neutrons escaping the target and number of the neutrons absorbed in the target and total neutron yield were calculated for different target radii. Results of these calculations are shown in Fig. 8. From this figure it can be seen that:
   (a) Total neutron yield increases with increasing target radius approaching a plateau value at high *R*-values.
   (b) Number of the neutrons escaping the target increases with increasing target radius reaching a maximum, beyond which it decreases with increasing target radius. In the case of the lead target, such a decrease is negligible for target radii up to 150 cm studied in this work. This is the consequence of the very low neutron absorption cross-section of lead as shown in Fig. 7.
   (c) As expected, the number of absorbed neutrons increases with increasing target radius. The rate of increase becomes smaller at large target radii to the extent that the absorption curves seem to level off (e.g. Fig. 8b and d).
   (d) In the cases of tungsten, thorium and uranium, the target radii corresponding to maximum number of the escaping neutrons were calculated by least square fits to the Monte Carlo results. In the case of the lead target the radius at which a *quasi-plateau* in the number of escaped neutrons starts is taken as the approximate radius corresponding to maximum number of neutron leakage from the Pb-target.

### 6.3. Irradiations with 1.5 GeV deuterons

Calculations given in Section 6.2 were repeated for 1.5 GeV deuterons and plots similar to those in Fig. 8 were obtained. As an example the results for the case of the $^{238}$U-target are shown in Fig. 9. It was found that:

(a) As for 1 GeV protons there is no gain in the number of escaping neutrons by increasing the target length beyond the range of the ions in the target material.
(b) The optimal target radii for the case of the 1.5 GeV deuterons are slightly larger than those for the case of the 1 GeV protons. Such an increase in the target radius is not obvious for the case of the lead target, because of the approximation involved in determination of the radius corresponding to maximum number of the escaping neutrons as discussed earlier (Fig. 8b).

Table 3 gives the optimal dimensions of the cylindrical targets of tungsten, lead, thorium and uranium for two projectile beams of 1 GeV protons and 1.5 GeV deuterons. Also given in Table 3 are the numbers of escaping neutrons per incident primary ion.

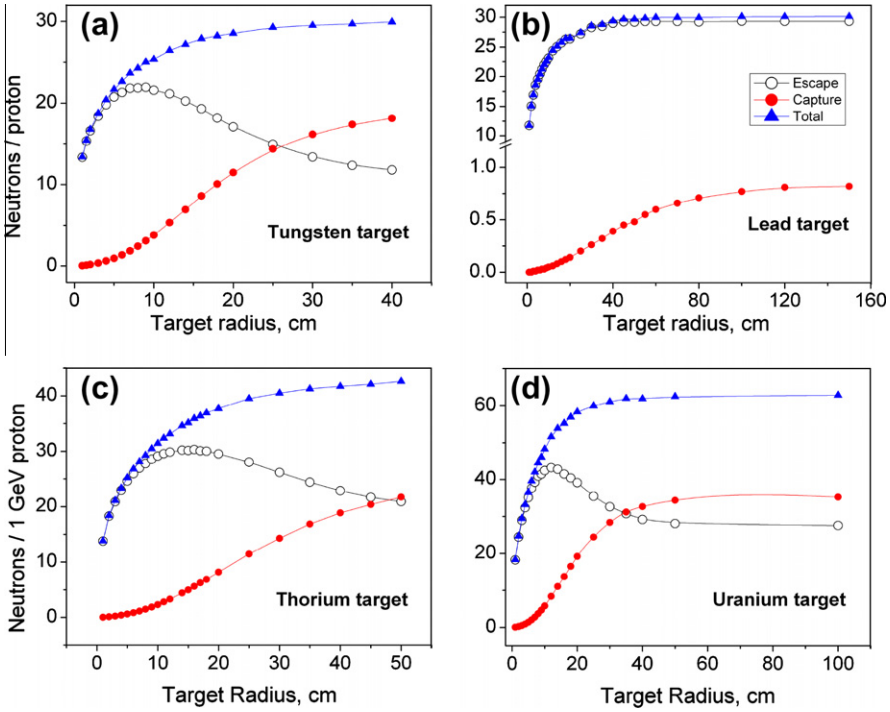


**Fig. 8.** Variation the escaping, captured and total neutron yield as function of the target radius in irradiation of range-long targets of $^{nat}W$, $^{nat}Pb$, $^{232}Th$ and $^{238}U$ with 1.0 GeV protons.

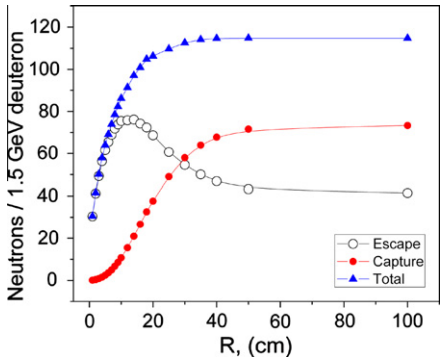


**Fig. 9.** Variations the escaping, captured and total neutron yield as function of the target radius in irradiation of a range-long target of $^{238}U$ with 1.5 GeV deuterons. The maximum number of escaping neutrons appears at a radius of 12.6 cm.

### 6.4. Dependence of the source neutron density and target size on ion beam size

#### 6.4.1. Beam size dependence of source neutron density

Numbers of escaping neutrons from an optimal cylindrical W-target (radius 8.6 and length 31 cm) on its irradiation with 1 GeV circular proton beams of different radii were calculated. Fig. 10a shows the variations of the total neutron yield and neutron leakage as a function of the proton beam radius.

As can be seen for a *fixed target radius*, neutron multiplicity decreases with increasing beam radius. Beam particles that interact with target nuclei at larger radii result in spallation neutrons that have greater chance of escaping the target than those produced at smaller radii. As a result the extent of their multiplication in internuclear cascade processes is reduced. Also in Fig. 10a variation of neutron leakage from the target (source neutrons) as a function of beam radius is shown. The leakage neutron number also decreases with increasing beam radius. In general this is expected, since the number of the leakage neutrons is expected to be proportional to the total number of neutrons produced.

#### 6.4.2. Beam size dependence of target size

Fig. 10a and the discussion given in Section 6.4.1, imply that the optimal target size also depends on the beam size. This is clearly shown in Fig. 10b. Neutron leakage from W-target of length 31 cm was calculated at different target radii ($R > 8.5$ cm) when it was irradiated with a proton beam of energy 1 GeV and radius 8.5 cm (corresponding to the last data point in Fig. 10a). In Fig. 10b the highest neutron leakage appears at a target radius of 11.2 cm as compared to 8.6 cm obtained for a beam radius of

**Table 3**
Optimal radius and length and number of the neutron leakage per incident ion for some cylindrical targets for 1 GeV proton and 1.5 GeV deuteron irradiations.

| Target material | 1 GeV proton | | | 1.5 GeV deuteron | | |
|---|---|---|---|---|---|---|
| | Radius (cm) | Length[a] (cm) | Escaping neutrons | Radius (cm) | Length[a] (cm) | Escaping neutrons |
| W | 8.6 | 31 | 22.0 | 9 | 42 | 38.2 |
| Pb[b] | ~60 | 54 | 29.3 | ~60 | 73 | 50.8 |
| Th | 14.2 | 54 | 30.2 | 15.8 | 73 | 51.2 |
| U | 11.7 | 34 | 43.1 | 12.6 | 45 | 72.6 |

[a] Target length is rounded up.
[b] Target radius for lead is approximate as seen in Fig. 8b.

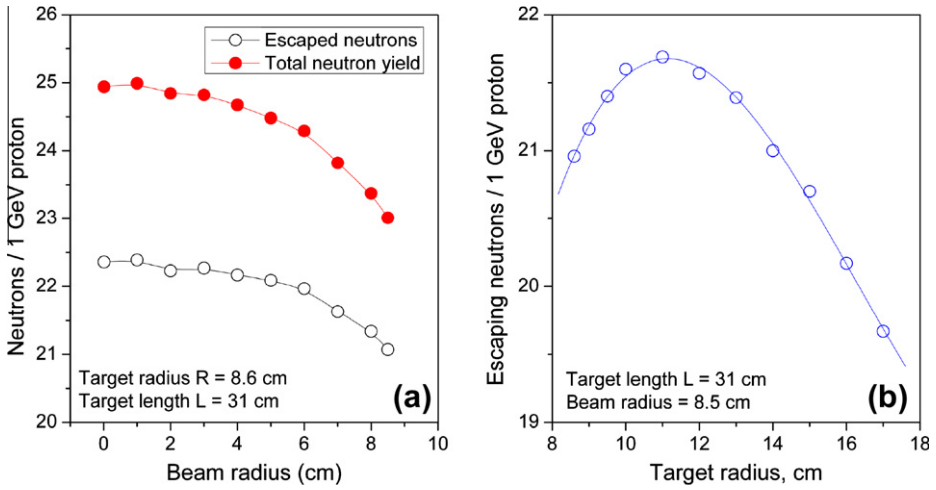


**Fig. 10.** (a) Variations of total neutron yield and neutron leakage from an optimal tungsten target with the incident beam radius on its irradiation with 1 GeV protons. Target dimensions are given in the figure inset. (b) Variation of neutron leakage from a tungsten target as a function of target radius. The target was irradiated with a proton beam of energy 1 GeV and radius 8.5 cm.

1 cm. Note that the maximum number of leakage neutrons is less than that for the case when a target of smaller radius (8.6 cm) was irradiated with a beam of 1 GeV protons with radius 1 cm (cf. Figs. 8 and 10a).

In practice the dependence of the target size on the beam size and shape will be much less pronounced. The proton or deuteron beams from accelerators is usually not circular, but in general the beam intensity shape can be approximated with Gaussian distributions along the *x*- and *y*-axes (the target being along the *z*-axis). Typically such distributions have FWHM in the range 1–3 cm, within which the majority (~77%) of the beam particles strike the target.

### 6.5. Target geometry

The most obvious target geometry is cylindrical because target material is then isotropically distributed around the incident ion beam axis. However, neutron yield from a square cuboid target with length and volume (and thus mass) equal to those of a cylindrical target was also examined (Fig. 11). The lengths of the both targets were equal to the range of the incident ions in the target material.

Although the surface area of the square cuboid target is ~11% more than its cylindrical equivalent, no significant difference in the number of the leakage neutrons were observed between these two target geometries. This observation provides flexibility in the design of ADS core.

## 7. Required beam current for an ADS

The energy gain of an ADS is given by the equation;

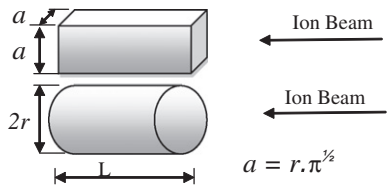


**Fig. 11.** Range-long square cuboid and cylindrical target geometries the same volume. On irradiation of these targets with ions along the central axis no significant difference on the number of the leakage neutrons were observed.

$$G = \chi_s \cdot \frac{\varphi^* k_{eff}}{\nu(1 - k_{eff})} \cdot E_f \tag{1}$$

where $\chi_s$ is the mean number of the neutrons that escape the target per incident primary ion, in units of neutrons per GeV, $k_{eff}$ is effective neutron multiplication factor of the sub-critical assembly in the absence of source neutrons, $\nu$ is the average number of neutrons released per fission, $E_f$ is the recoverable energy released per fission (in units of GeV) and $\varphi^*$ is the importance of the source neutrons (Salvarores et al., 1997). Obviously the energy gain $G$, refers to thermal output power of the ADS.

The neutron importance $\varphi^*$ for spallation neutron driven systems with $G > 1$ is a quantity greater than unity and it arises from the deviation of the source neutron spectrum from that of fission neutrons which are well described by Watt spectrum. In addition to fission reactions, high-energy spallation neutrons escaping the target can multiply within the ADS medium by other means such as (n, xn) reactions.

The accelerator beam current $I$ (in units of mA) for thermal output power of an ADS, $(P_o)_{\text{th}}$ (in units of $MW_{\text{th}}$) is given by

$$(P_o)_{\text{th}} = I \cdot E_i \cdot G \tag{2}$$

where $E_i$ is incident ion energy in units of GeV.

Fraction $f$, of the output power of the ADS that is required to operate the coupled accelerator is given by:

$$f = \frac{1}{G\eta\varepsilon} \tag{3}$$

where $\eta$ is the thermal power to electric power conversion efficiency (thermodynamic efficiency) and $\varepsilon$ is the electric power to beam power conversion efficiency.

Let us consider an ADS with $k_{eff} = 0.98$. We calculate the required beam power for a thermal output power of 1.5 $GW_{\text{th}}$. Using Eq. (1) and assuming $\nu = 2.5$ and $E_f = 0.2$ GeV we calculate the energy gain for the four cases; tungsten, lead, thorium and uranium targets each irradiated with 1 GeV proton and 1.5 GeV deuteron projectiles.

Table 4 gives the source neutron yield per ion, $Y$, and escaping neutrons per unit energy of the incident ion (neutrons/GeV), $\chi_s$, from optimal targets of $^{\text{nat}}$W, $^{\text{nat}}$Pb, $^{232}$Th and $^{238}$U when they are irradiated by 1 GeV proton and 1.5 GeV deuteron beams. Table 4 also shows the energy gain $G$, the required beam current for an output power of 1.5 $GW_{\text{th}}$ for each of the target projectile systems, as well as the increase in gain when the proton beam is replaced

**Table 4**
The energy gain and required accelerator beam current for an ADS with $k_{eff}$ = 0.98 with optimal targets of $^{nat}$Pb, $^{nat}$W, $^{232}$Th and $^{238}$U when they were irradiated by 1 GeV proton and 1.5 GeV deuteron beams. The required beam current represent lower and upper limits, respectively (see the text for detail).

| Ion + target | $E_i$ (GeV) | $Y$ source neutrons per ion | $\chi_s$ neutrons/GeV | $G$ energy gain | Required beam current for output power of 1.5 $GW_{th}$ (mA) | $(G_d - G_p)/G_p$ (%) | $f$ (%) |
|---|---|---|---|---|---|---|---|
| p + $^{nat}$W | 1 | 22.0 | 22.0 | 86.2 | 17.4 | 15.8 | 6.4 |
| d + $^{nat}$W | 1.5 | 38.2 | 25.5 | 99.8 | 10.0 | | 5.6 |
| p + $^{nat}$Pb | 1 | 29.3 | 29.3 | 114.9 | 13.1 | 15.6 | 4.8 |
| d + $^{nat}$Pb | 1.5 | 50.8 | 33.9 | 132.8 | 7.5 | | 4.2 |
| p + $^{232}$Th | 1 | 30.2 | 30.2 | 118.4 | 12.7 | 12.5 | 4.7 |
| d + $^{232}$Th | 1.5 | 51.2 | 34.1 | 133.7 | 7.5 | | 4.2 |
| p + $^{238}$U | 1 | 43.1 | 43.1 | 169.0 | 8.9 | 10.8 | 3.3 |
| d + $^{238}$U | 1.5 | 72.6 | 48.4 | 189.8 | 5.3 | | 3.0 |

with a deuteron beam $[(G_d - G_p)/G_p]$. The last column gives the fraction of the output power, required to operate the accelerator coupled to the sub-critical system, assuming that $\eta = 0.45$ and $\varepsilon = 0.4$ (Fernandez et al., 1996; Rubbia et al., 1995) (these efficiency factors seem rather generous, however their values do not alter the conclusions of this paper). In these calculations we have used a value of $\varphi^* = 1$, therefore the obtained energy gains and the required currents represent lower and upper limits, respectively.

From Table 4 it is evident that by using 1.5 GeV deuteron beams instead of 1 GeV protons, the increased energy gain, and thus the output power is higher (by a factor of 2.8–3.6) than the power required to operate the coupled accelerator, in all four target materials studied.

As already mentioned, because of the assumption of $\varphi^* = 1$ the energy gain values given in Table 4 are lower limit values and the beam currents are upper value estimates. To have an estimate of the effects of the neutron importance $\varphi^*$ additional calculations were made.

### 7.1. Effects of neutrons from non-fission events on the required beam current

So far calculations are restricted to neutrons produced within the target volume and the source neutrons are defined as those that escape the target. This is equivalent to the assumption that outside the target, neutrons are produced only by means of fission in the ADS fuel system. In other words the neutrons with non-fission origins resulting from the interaction of the source neutrons with the moderator, structural and fuel materials are ignored.

Fig. 12a shows the spectrum of the neutrons that escape the target and enter the ADS volume when a $^{238}$U-target of optimal size is irradiated with a beam of 1.5 GeV deuterons. In Table 5 neutron

**Table 5**
Leakage neutrons from $^{238}$U-target when irradiated with a beam of 1.5 GeV deuterons.

| Energy interval | Neutrons/ion (%) |
|---|---|
| $E_n \leqslant 1$ keV | 2.46E−03 |
| 1 keV < $E_n \leqslant$ 1 MeV | 73.33 |
| 1 MeV < $E_n \leqslant$ 30 MeV | 24.93 |
| $E_n$ > 7.5 MeV | 4.56 |
| $E_n$ > 30 MeV | 1.73 |

abundances are assigned to different energy groups. The neutron induced fission cross-section of lead becomes significant at energies above 30 MeV and the weighted mean threshold energy for $^{nat}$Pb(n, xn) is ~7.5 MeV. It can be seen that neutron energies extend to several hundred MeV and thus in an ADS these neutrons can produce extra neutrons in interactions with material beyond the target.

As an example, an optimal uranium target was placed in the centre and along the axis of a cylindrical container of both diameter and height of 3 m. On irradiation of the target with 1.5 GeV deuterons along its axis, 72.6 neutrons/deuteron escape the target and enter the volume of the tank (these are the source neutrons). Now one may fill the tank with natural lead and the target becomes embedded in the lead. Calculations show that by interaction of the *source neutrons* with the material in the tank ($^{nat}$Pb in this case) an extra 7.84 neutrons are produced via (n, xn) reactions, which is about 11% of the number of source neutrons.

Calculation showed that, when the $^{nat}$Pb in the container is replaced with LBE (44.5 wt.% $^{nat}$Pb + 55.5 wt.% Bi) 7.78 neutrons are produced via (n, xn) reactions, which is the same as that for the

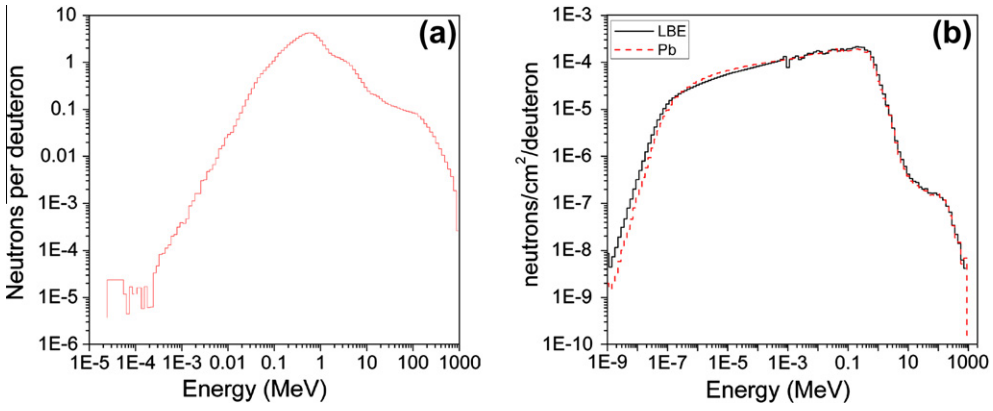


**Fig. 12.** (a) Energy spectrum of the neutrons escaping optimal uranium target when it is irradiated with 1.5 GeV deuterons parallel to its axis. (b) Average neutron spectrum in $^{nat}$Pb and LBE surrounding a $^{238}$U-target of optimal size when it was irradiated with 1.5 GeV deuterons. The U-target was located at the centre and along the axis of a cylindrical tank of diameter and height 3 m filled with $^{nat}$Pb or LBE.

**Table 6**
The required beam current for different output powers for a lead moderated ADS ($k_{eff}$ = 0.98) with $^{nat}$Pb or $^{238}$U-target when 1 GeV proton or 1.5 GeV deuteron beams are used.

| Output power ($MW_{th}$) | Output power ($MW_e$)[a] | Average ion beam current (mA) | |
|---|---|---|---|
| | | *p* (1 GeV) + Pb system | *d* (1.5 GeV) + U system |
| 222 | 100 | 1.9 | 0.7 |
| 555 | 250 | 4.6 | 1.8 |
| 1111 | 500 | 9.3 | 3.5 |
| 1500 | 675 | 12.5 | 4.8 |
| 2222 | 1000 | 18.5 | 7.1 |

[a] A thermodynamic efficiency of 0.45 was used to convert the thermal to electric power (Fernandez et al., 1996; Rubbia et al., 1995).

case of the $^{nat}$Pb moderator. This is due to the facts that (i) the average threshold energy for (n, 2n) reaction for LBE and $^{nat}$Pb is almost the same (~7.5 MeV) and (ii) the average neutron spectrum in the tank for the case of the $^{nat}$Pb and LBE is very similar as shown in Fig. 12b.

In a nuclear assembly, including an ADS, neutrons mainly multiply via fission events induced by secondary and fission neutrons. In the case of fissionable nuclei, such as uranium isotopes, neutron multiplication via fission is handled quite smoothly by neutron transport codes such as MCNPX in the energy range where data tables are available. However, in the case of other nuclei such as lead, neutrons resulting from *high-energy secondary neutron* induced fission and their contribution to neutron multiplication is not readily obtainable from the neutron transport codes. This is mainly because of lack of the relevant nuclear data tables for these isotopes.

Cross-sections for neutron induced fission for tungsten, lead and bismuth are dramatically less than those of thorium and uranium at the relevant energies (Prokofiev, 2001a). Moreover, the thresholds for neutron induced fission in tungsten, lead and bismuth are much higher than those in $^{232}$Th and $^{238}$U. Furthermore, from Fig. 12b it can be seen that number of neutrons with energy greater than 30 MeV (energy relevant to the fission of Pb and Bi) is only ~0.02% of the total neutrons in the Pb or LBE moderators. Therefore we conclude that the contribution of the secondary neutron induced fission in the lead or LBE to the neutron multiplication in the system is negligible and can be safely ignored.

Table 6 gives the average beam current for different output powers for a lead moderated ADS ($k_{eff}$ = 0.98) with lead or uranium target when 1 GeV proton or 1.5 GeV deuteron beams are used. The required beam current for the (1.5 GeV d + U) system is 2.6 times lower than the current required for the (1 GeV p + Pb) system when identical output power is reached. It must be noted that the beam currents given in the table are approximate and will be different if the material content of the ADS is changed.

For a modular ADS with output power of 250 $MW_e$ (equivalent to 550 $MW_{th}$) and a uranium target, a deuteron beam of current 1.8 mA is required, which is achievable with today's technology. For 1 $GW_e$ (2.2 $GW_{th}$) for (1 GeV p + Pb) system the required current is 18.5 mA and for (1.5 GeV d + U) system it is only 7.1 mA.

## 8. Technical issues related to target materials and deuteron beam

### 8.1. Lead or LBE target

To obtain maximum neutron yield from a Pb-target an optimal target radius of ~60 cm is required which is too large and will result in physical and technical difficulties in utilization of the produced neutrons. Thus, use of Pb-target makes sense only when the neutron moderating environment is also lead and the spallation process has enough physical space to complete. This condition applies only for the case of fast ADS. Use of smaller target radius in slow ADS will result in loss of the potential output power.

### 8.2. Uranium and thorium targets

Extended uranium spallation target has been studied experimentally by several groups, e.g. (Adam et al., 2010; Andriamonje et al., 1995; Wan et al., 2001). In the FEAT experiment of the CERN a small depleted uranium target has been used (Andriamonje et al., 1995). The FEAT sub-critical assembly had an effective neutron multiplication factor of $k_{eff} = 0.895 \pm 0.010$ and an energy gain of $29 \pm 2$. From Eq. (1), one obtains $\chi_s\varphi^* = 41.7$. At proton energy of 1 GeV, 43.1 neutrons escape the optimal uranium target (Table 3). As $\varphi^* > 1$ then in the FEAT experiment number of the neutrons escaping the target must have been less than 41.7 which is consistent with small size of the uranium target that was used in the experiment. The 41.7 neutrons per 1 GeV proton are in fact total number of neutrons resulting from the interaction of the projectile with target nuclei and all other interactions of the secondary particles with the material in the sub-critical assembly, except those produced by secondary neutron induced fission events in the fuel.

Uranium and thorium targets differ from W, Pb and LBE targets in two major aspects;

1. Relatively high fission cross-section and thus fission heating of the target
2. Transmutability to fissile materials

#### 8.2.1. Relatively high fission cross-section of $^{238}$U and fission heating of the target

Detailed studies of spallation reactions by (Bernas et al., 2003) and (Enqvist et al., 2001) show that for thin target interactions the fission cross-section for 1 AGeV $^{238}$U + p and 1 AGeV $^{208}$Pb + p are $1.53 \pm 0.13$ b and $0.16 \pm 0.07$ b, respectively. The total interaction cross-sections for these two reactions are almost the same, $1.99 \pm 0.17$ b for $^{238}$U and $1.84 \pm 0.23$ b for $^{208}$Pb. Therefore in the interaction of 1 GeV protons with an uranium target the dominant reaction mode is fission while in the case of the lead target fragmentation is the main reaction channel.

In a thick target (longer than the range of the ions) the number of primary ion-induced fission reactions in the target can be calculated via the following equation;

$$N_f = N\int_0^{R_i - R_{th}} \sigma_f(x)F(x)dx = N\int_{E_i}^{E_{th}} \frac{\sigma_f(E)F(E)}{S(E)}dE, \quad (4)$$

where $x$ is the length along the incident ion trajectory in the target at which the ion energy is reduced from incident energy of $E_i$ to $E$, $N_f$ is fissions per unit volume of the target, $N$ is the number of target nuclei per unit volume, $\sigma_f(E)$ is the fission cross-section at energy $E$ (corresponding to distance $x$ in the target), $F(E)$ is the energy dependent time integrated fluence of the incident ions, $S(E) = dE/dx$ is the energy dependent stopping power of the ion in the target medium, $E_{th}$ is the threshold energy for induced fission in target nuclei, $R_i$ is the range of the ions in the target material and $R_{th}$ is the range corresponding to the threshold energy $E_{th}$. Detailed knowledge of the energy dependent fission cross-section for deuteron-induced fission in uranium and lead in the energy range of GeV to $E_{th}$ is not available. However, proton induced fission cross-sections and stopping powers may be obtained from Prokofiev (2001b) and Ziegler et al. (1985), respectively.

In the light of the facts noted above, the primary ion-induced fission in a uranium target will be at least an order of magnitude higher than that in a lead or LBE target.

Moreover in an optimal $^{238}$U-target located at the centre of a cylindrical tank of diameter and height 3 m filled with Pb or LBE, on average 12.85 fissions per incident deuteron of energy 1.5 GeV, are induced by secondary neutrons. Of these 11.85 fissions are caused directly by secondary neutrons in the target and one fission is induced by the neutrons that reflect from the surrounding LBE into the target. These fission events deposit 2.2 GeV energy in the target via fission fragments (assuming a total kinetic energy of 170 MeV for the uranium fission fragments). This is about 1.5 times of the energy of the incident deuterons, i.e. an energy gain of ~1.5 will be obtained just by the secondary neutron induced fissions in the target. In other words for an average beam current of 1 mA (beam power of 1.5 $MW_{th}$) 2.2 $MW_{th}$ power will be deposited in the target solely by the secondary neutron induced fissions in the target. For W, Pb and LBE the *secondary neutron induced fission* and corresponding fission heating will not be significant as discussed earlier.

Therefore if a U-target was used in an ADS, a special cooling mechanism must be present for fast removal of the extensive and localized heat from the target region.

### 8.2.2. Transmutability to fissile materials

In the course of ADS operation, transmutation of uranium in a uranium target to Pu-isotopes and thorium in a thorium target to $^{233}$U nuclei is expected to alter source neutron yield because of creation of new fissionable materials in the target medium. Thus in an ADS with uranium or thorium target, appropriate allowances must be made for these new materials in the system.

### 8.2.3. Nuclear waste inventory of the spallation targets

Spallation reactions result in production of radioactive residues in the target regardless of the type of target material. Inverse kinematics nuclear reaction studies carried out in GSI give details of the isotopes (spallation residues) produced in interaction of lead and uranium with protons in *thin* targets. In Table 7 the charge and mass number ranges of the evaporation and fission residues are given for the Pb + p and U + p reactions.

In the case of the lead target evaporation residue will be much more than the fission residue, while for the uranium target the opposite will be the case.

In a thick target an example of long-lived nuclear waste material that will be produced in a U-target is $^{237}$Np. In the U + p reaction the evaporation residue $^{237}$U is produced with relatively high cross-section of 68.7 mb (Taïeb et al., 2003) via $^{238}$U(p, pn) reaction. In the case of the U + d reaction it will be produced through (d, p2n) reaction. In thick uranium targets, $^{237}$U will be formed via $^{238}$U(n, 2n) reactions as well. Beta decay of $^{237}$U with half-life of 6.75 d will result in production of $^{237}$Np which is a long-lived (2.14 My) alpha emitting nuclear waste material. In the intense spallation neutron field within the target and in the neutron field of the ADS as a whole, large fraction of produced $^{237}$Np will be destroyed via $^{237}$Np(n, f) or transmuted to $^{238}$Np (Wan et al., 2001; Westmeier et al., 2005) and eventually to Pu and to some minor actinide nuclei. It is worth mentioning that $^{238}$Np has very high fission cross-section of about 2000b for thermal neutrons which reduces to ~2 b at neutron energy of 20 MeV. It is expected that, the large fraction of the Pu and minor actinides also to be destroyed via fission (Hashemi-Nezhad et al., 2002b; Revol, 1999; Rubbia et al., 1997).

In a 1.5 GeV deuteron operated ADS with an optimal U-target, total target mass will be 426 kg. At the end of the target life-time, one will have significantly less than 426 kg of waste material (not all target nuclei will be long-lived radioactive species).

Most of the future ADSs are expected to be designed and used for nuclear waste transmutation, see e.g. (Cinotti et al., 2004). In such cases massive amount of highly radiotoxic material will be injected inside ADS either as part of the fuel system (a MOX fuel operated ADS, see e.g. Calgaro et al., 2008; Shvetsov et al., 2006) or just for transmutation purposes. Presence of couple of hundred kilograms of waste material in the system (majority of which will be fission products) is not expected to be a major issue.

The above given facts and arguments must be completed with detailed burn-up studies and calculations of the uranium and thorium targets. Such studies also will be relevant to the transmutation of $^{238}$U and $^{232}$Th to fissile materials (as was discussed in Section 8.2.2).

## 8.3. Radiation damage

In principle a thorium or uranium target must have a leak proof housing to prevent the mixing of fission and spallation residues (generally radioactive isotopes) with the other materials within the ADS. This is also a preferred option for any other types of spallation targets. The spallation target housing arrangement must allow easy and safe extraction of the gaseous products from the target assembly. The latter issue is not unique to thorium and uranium targets and is applicable to any other spallation neutron targets including lead and LBE.

For years uranium with appropriate cladding has been used as nuclear fuel in the form of fuel elements/bundles. The same technology can be extended to uranium ADS target, with the difference that a uranium target is continuously bombarded with relativistic particles which results in creation of massive amounts of radiation damage within the target volume and its housing.

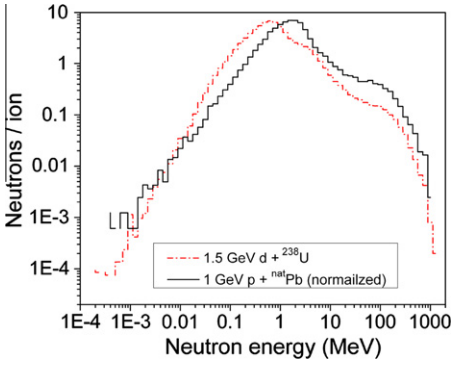


**Fig. 13.** Spectra of the source neutrons from $^{238}$U and $^{nat}$Pb-targets when they were irradiated with 1.5 GeV deuteron and 1 GeV proton, respectively. The area under the both spectra is the same and the spectrum of the neutrons from $^{nat}$Pb-target is normalized to that from the $^{238}$U-target.

**Table 7**
Charge and mass number ranges of the evaporation and fission residues for Pb + p and U + p reactions.

| Spallation reaction | Evaporation residues | | | Fission fragments | | |
|---|---|---|---|---|---|---|
| | *Z* | *A* | Reference | *Z* | *A* | Reference |
| Pb + p at 0.5 AGeV | 69–83 | 164–208 | (Audouin et al., 2006) | 23–56 | 50–136 | (Fernández-Domínguez et al., 2005) |
| Pb + p at 1.0 AGeV | 61–82 | 132–207 | (Enqvist et al., 2001) | 22–52 | 47–127 | (Enqvist et al., 2001) |
| U + p at 1.0 AGeV | 74–92 | 165–237 | (Taïeb et al., 2003) | 28–75 | 61–184 | (Bernas et al., 2003, 2006) |

In Fig. 13 the spectra of the source neutrons for 1.5 GeV d + $^{238}$U and 1 GeV p + $^{nat}$Pb projectile target systems are shown. The spectrum for 1 GeV p + $^{nat}$Pb system is normalized to that of the 1.5 GeV d + $^{238}$U and as a result the areas under the spectra are equal. As can be seen the spectrum of the source neutrons form 1 GeV p + $^{nat}$Pb system is harder than that of 1.5 GeV d + $^{238}$U, mainly because of the contribution of fission neutrons to the latter. Thus, for the same output powers of the ADS the spallation neutron induced radiation damage in the target housing will be higher for a lead target than that for a uranium target. Studies related to the material selection of the spallation beam windows, see e.g. (Sordo et al., 2009) can provide valuable information on selection of the material for spallation target housing.

### 8.4. High-power deuteron accelerator

For an industrial scale ADS a high-power ion accelerator is required. To exploit the advantages that a deuteron beam provides (as illustrated in this work) it is required to couple the sub-critical assembly to a high-power deuteron accelerator with average beam current of several mA. Recent works of (Antipov et al., 2008; Demchenko et al., 2006; Ferdinand et al., 2002) show that there is no technical problem with the ions source and low energy part of a high current deuteron accelerators. Work of (Ferdinand et al., 2002) shows that a beam current of 250 mA at 40 MeV is achievable.

## 9. Conclusions

On irradiation of different targets with ions in the range of $Z = 1$ to $Z = 82$ and energy 1 AGeV, neutron production rate, NPR (neutron yield/GeV) is highest for projectiles of hydrogen isotopes. Systematic dependences using a lead target as an example are presented in this paper. Four target types of $^{nat}$W, $^{nat}$Pb, $^{232}$Th and $^{238}$U were studied in more detail because of their high values of NPR as compared with other target materials (Sections 3 and 4).

Calculations show that the deuteron is a superior projectile to the proton. Regardless of the type of target material, spallation neutron production rate for deuteron projectiles is higher than that for protons of the same kinetic energy (Fig. 4). For both ions the NPR rises sharply with increasing ion energy, reaching a maximum beyond which it decreases slowly with increasing ion energy. It is shown that the reduction of the NPR at energies beyond the energy corresponding to the maximum NPR, (for targets with length larger than the particle range), is the consequence of the reduction in inelastic interaction cross-section of the projectile with the target nuclei (Section 5).

For spallation targets the source neutrons are defined as those that escape the target and are produced by interactions of the primary ions and resulting secondary particles, prior to their escape from the target, with the target nuclei. With this definition the optimal target size refers to target dimensions where for a given incident ion energy the largest number of neutrons escape the target surfaces. On the basis of this definition optimal target sizes for $^{nat}$W, $^{nat}$Pb, $^{232}$Th and $^{238}$U-targets on their irradiation with 1 GeV protons and 1.5 GeV deuterons were calculated and are presented in Table 3 (Sections 6.1–6.3). It is shown that optimal target size can be affected by beam size (shape) and for increased beam sizes the optimal target size is larger (Section 6.4.2).

By changing the geometry of the range-long target from cylindrical to a square cuboid of the same volume, no significant difference in the number of leakage neutrons was observed (Section 6.5).

It is shown that the energy gain for (1.5 GeV d + U) system is significantly higher than that for (1 GeV p + Pb), which is the generally accepted projectile target combination for an ADS. The higher energy gain of the (1.5 GeV d + U) system results in reduction of the coupled accelerator current by a factor of ~2.6. This has major technological and economical significance and facilitates the implementation of an industrial scale ADS (Section 7).

The high fission rate in a uranium target will result in extensive heating of the target as compared to Pb or LBE targets. Therefore when U-target is used a special cooling mechanism must be operational to remove the extensive and localized heat from the target region (Section 8.2.1).

As the neutron spectrum from a 1.5 GeV d + U system is softer than that of a 1 GeV p + Pb system, the use of uranium as an ADS target will not introduce extra complications (compared with the case of a Pb-target) regarding spallation neutron induced radiation damage (Section 8.3).

## References


Aarnio, P.A. et al., 1986. FLUKA-86 Users Guide. CERN TIS-RP/186.

Adam, J., et al., 2002. Transmutation of 239-Pu and other nuclides using spallation neutrons produced by relativistic protons reacting with massive U- and Pb-targets. Radiochimica Acta 90, 431–442.

Adam, J., et al., 2010. Studies of deep subcritical electronuclear systems and feasibility of their application for energy production and radioactive waste transmutation. E1-2010-61, Joint Institute for Nuclear Research, Dubna, Russia.

Andriamonje, S. et al., 1995. Experimental determination of the energy generated in nuclear cascades by a high energy beam. Physics Letters B 348, 697–709.

Antipov, Y., et al., 2008. Deuteron beam accelerator at LINAC I-100 and IHEP. In: Proceedings of RuPAC 2008. Zvenigorod, Russia.

Atchison, F., 1980. Spallation and fission in heavy metal nuclei under medium energy proton bombardment. In: Targets for Neutron Beam Spallation Sources. Targets for Neutron Beam Spallation Sources, Jul-Conf-34, Kernforschungsanlage Julich GmbH, January, 1980.

Audouin, L. et al., 2006. Evaporation residues produced in spallation of $^{208}$Pb by protons at. Nuclear Physics A 768, 1–21.

Barashenkov, V.S., Toneev, V.D., Chigrinov, S.E., 1974. Interaction of high-energy deuteron beams in matter. Atomic Energy 37, 480–483.

Barish, J., et al., 1981. HETFIS High-energy Nucleon–Meson Transport Code with Fission. Oak Ridge National Laboratory Report ORNL-TM-7882, July, 1981.

Bernas, M. et al., 2003. Fission-residues produced in the spallation reaction $^{238}$U + p at 1 A GeV. Nuclear Physics A 725, 213–253.

Bernas, M. et al., 2006. Very heavy fission fragments produced in the spallation reaction $^{238}$U+p at 1 A GeV. Nuclear Physics A 765, 197–210.

Bertini, H.W., 1963. Low-energy intranuclear cascade calculation. Physical Review 131, 1801–1821.

Bertini, H.W., 1969. Intranuclear-cascade calculation of the secondary nucleon spectra from nucleon–nucleus interactions in the energy range 340 to 2900 MeV and comparisons with experiment. Physical Review 188, 1711–1730.

Boudard, A., Cugnon, J., Leray, S., Volant, C., 2002. Intranuclear cascade model for a comprehensive description of spallation reaction data. Physical Review C 66, 044615.

Bowman, C.D. et al., 1992. Nuclear energy generation and waste transmutation using an accelerator-driven intense thermal neutron source. Nuclear Instruments and Methods A 320, 336–367.

Calgaro, B., Vezzoni, B., Cerullo, N., Forasassi, G., Verboomen, B., 2008. Wastes Management through Transmutation in an ADS Reactor. Science and Technology of Nuclear Installations Article ID 756181. doi:10.1155/2008/756181.

Carminati, F., et al., 1993. An Energy Amplifier for Cleaner and Inexhaustible Nuclear Energy Production Driven by a Particle Beam Accelerator. CERN/AT/93-47.

Chadwick, M.B. et al., 1999. Cross section evaluations to 150 MeV for accelerator-driven systems and implementation in MCNPX. Nuclear Science and Engineering 131, 293.

Cinotti, L., Giraud, B., Abderrahim, H.A., 2004. The experimental accelerator driven system (XADS) designs in the EURATOM 5th framework programme. Journal of Nuclear Materials 335, 148–155.

Demchenko, P.O. et al., 2006. A deuteron LINAC for subcritical assembly driving. Problems of atomic science and technology. Nuclear Physics Investigations 47, 34–36 (No. 3. Series).

Dresner, L., 1981. EVAP-A Fortran Program for Calculating the Evaporation of Various Particles from Excited Compound Nuclei, Oak Ridge National Laboratory, ORNL-TM-7882, July 1981.

Enqvist, T. et al., 2001. Isotopic yields and kinetic energies of primary residues in 1 A GeV $^{208}$Pb+p reactions. Nuclear Physics A 686, 481–524.

Ferdinand, R., et al., 2002. Deuteron beam test for IFMIF. In: Proceedings of EPAC 2002. Paris, France.

Fernández-Domínguez, B. et al., 2005. Nuclide cross-sections of fission fragments in the reaction $^{208}$Pb + p at 500 A MeV. Nuclear Physics A 747, 227–267.

Fernandez, R., Mandrillon, P., Rubbia, C., Rubio, J.A., 1996. A Preliminary Estimate of the Economic Impact of the Energy Amplifier. Preprint. CERN/LHC/96-01-EET.

Hashemi-Nezhad, S.R. et al., 2001. Monte Carlo analysis of accelerator driven systems; studies on spallation neutron yield and energy gain. Kerntechnik 66, 47–53.

Hashemi-Nezhad, S.R. et al., 2002. Monte Carlo calculations on transmutation of transuranic nuclear waste isotopes using spallation neutrons; difference of lead and graphite moderators. JINR Report E1-2001-44. Nuclear Instruments and Methods A 482, 537–546.

Junghans, A.R., Jong, et al., 1998. Projectile-fragment yields as a probe for the collective enhancement in the nuclear level density. Nuclear Physics A 629, 635–655.

Lone, M.A., Wong, P.Y., 1995. Neutron yield from proton-induced spallation reactions in thick targets of lead. Nuclear Instruments and Methods in Physics Research A 362, 499–505.

Mashnik, S.G., et al., 2006. CEM03.S1, CEM03.G1, LAQGSM03.S1, and LAQGSM03.G1 Versions of CEM03.01 and LAQGSM03.01 Event-Generators. Los Alamos National Laboratory Report LA-UR-06-1764, March 6, 2006.

NEA, 2007. Handbook on Lead–bismuth Eutectic Alloy and Lead Properties, Materials Compatibility, Thermal-hydraulics and Technologies. Atomic Energy Agency. <http://www.nea.fr/science/reports/2007/pdf/chapter2.pdf>.

Pelowitz, D.B., 2008. MCNPX User's Manual Version 2.6.0, LA-CP-07-1473, April 2008.

Pelowitz, D.B., et al., 2008. MCNPX 2.7.A Extensions (beta version), LA-UR-08-07182. Los Alamos National Laboratory.

Prael, R.E., Lichtenstein, H., 1989. User Guide to LCS: The LAHET Code System, Report No. LA-UR-89-3014. Los Alamos National Laboratory.

Prokofiev, A., 2001a. Nucleon-induced Fission Cross Sections of Heavy Nuclei in the Intermediate Energy Region. Doctor of Philosophy Thesis: Uppsala University. ISBN 91-554-5009-1.

Prokofiev, A.V., 2001b. Compilation and systematic of proton-induced fission cross-section data. Nuclear Instruments and Methods A 463, 557–575.

Revol, J.-P., 1999. The TARC Experiment (PS211): Neutron-driven Nuclear Transmutation by Adiabatic Resonance Crossing. CERN 99-11, 1999.

Ridikas, D., Mittig, W., 1998. Neutron production and energy generation by energetic projectiles: protons or deuterons? Nuclear Instruments and Methods in Physics Research A 418, 449–457.

Rubbia, C., Buono, S., Kadi, Y., Rubio, J.A., 1997. Fast Neutron Incineration in the Energy Amplifier as Alternative to Geological Storage: The Case of Spain. CERN/LHC/97-01.

Rubbia, C., et al., 1995. Conceptual Design of a Fast Neutron Operated High Power Energy Amplifier. CERN/AT/95-44 (ET).

Salvarores, M. et al., 1997. The potential of accelerator-driven systems for transmuatation or power production using thorium or uranium fuel cycles. Nuclear Science and Engineering 126, 333–340.

Shvetsov, V. et al., 2006. The subcritical assembly in Dubna (SAD) – part I: coupling all major components of an accelerator driven system (ADS). Nuclear Instruments and Methods in Physics Research A 562, 883–886.

Sordo, F. et al., 2009. Material selection for spallation neutron source Windows application to PDS-XADS and XT-ADS prototypes. Nuclear Engineering and Design 239, 2573–2580.

Taïeb, J. et al., 2003. Evaporation residues produced in the spallation reaction $^{238}$U+p at 1 A GeV. Nuclear Physics A 724, 413–430.

Vassilkov, R.G., Myzin, N.S., Chirkin, T.M., 1995. Neutron yield from a massive lead target under the action of relativistic light ions. Atomic Energy 79, 664–670.

Wan, J.-S. et al., 2001. Transmutation of $^{129}$I and $^{237}$Np using spallation neutrons produced by 1.5, 3.7 and 7.4 GeV protons. Nuclear Instruments and Methods in Physics Research A 463, 634–652.

Westmeier, W. et al., 2005. Transmutation experiments on I-129, La-139 and Np-237 using the nuclotron accelerator. Radiochemica Acta 93, 65–73.

Yariv, Y., Fraenkel, Z., 1979. Intranuclear cascade calculation of high-energy heavy-ion interactions. Physical Review C 20, 2227–2243.

Yariv, Y., Fraenkel, Z., 1981. Intranuclear cascade calculation of high energy ion collisions: effect of interactions between cascade particles. Physical Review C 24, 488–494.

Yurevich, V.I., 2010. Production of neutrons in thick targets by high energy protons and nuclei. Physics of Particles and Nuclei 41, 778–825.

Yurevich, V.I. et al., 2006. Investigation of neutron emission in the interaction of relativistic protons and deuterons with lead targets. Physics of Particles and Nuclei Letters 3, 169–182.

Ziegler, J.F., Biersack, J.P., Littmark, U., 1985. The Stopping and Range of Ions in Matter. Pergamon Press. <http://www.SRIM.org>.